



HAL
open science

Compressive failure of composites: A computational homogenization approach

Saeid Nezamabadi, Michel Potier-Ferry, Hamid Zahrouni, Julien Yvonnet

► To cite this version:

Saeid Nezamabadi, Michel Potier-Ferry, Hamid Zahrouni, Julien Yvonnet. Compressive failure of composites: A computational homogenization approach. *Composite Structures*, 2015, 127, pp.60-68. 10.1016/j.compstruct.2015.02.042 . hal-01134132

HAL Id: hal-01134132

<https://hal.science/hal-01134132v1>

Submitted on 10 Mar 2016

HAL is a multi-disciplinary open access archive for the deposit and dissemination of scientific research documents, whether they are published or not. The documents may come from teaching and research institutions in France or abroad, or from public or private research centers.

L'archive ouverte pluridisciplinaire **HAL**, est destinée au dépôt et à la diffusion de documents scientifiques de niveau recherche, publiés ou non, émanant des établissements d'enseignement et de recherche français ou étrangers, des laboratoires publics ou privés.

Compressive failure of composites: A computational homogenization approach

Saeid Nezamabadi^a, Michel Potier-Ferry^{b,*}, Hamid Zahrouni^b, Julien Yvonnet^c

^a*Université Montpellier 2, Laboratoire de Mécanique et Génie Civil, UMR CNRS 5508, CC048 Place Eugène Bataillon, 34095 Montpellier Cedex 05, France*

^b*Université de Lorraine, Laboratoire d'Etude des Microstructures et de Mécanique des Matériaux, UMR CNRS 7239, Ile du Saulcy 57045, Metz Cedex 01 France*

^c*Université Paris-Est, Laboratoire Modélisation et Simulation Multi Échelle, UMR CNRS 8208, 5 Bd Descartes, 77454 Marne-la-Vallée Cedex 2, France*

Abstract

This paper revisits the modeling of compressive failure of long fiber composite materials by considering a multiscale finite element approach. It is well known that this failure follows from a fiber microbuckling phenomenon. Fiber microbuckling is governed by both material and geometrical quantities: the elastoplastic shear behavior of the matrix and the fiber misalignment. Although all these parameters are easily accounted by a finite element analysis at the local level, the failure is also influenced by macrostructural quantities. That is why a multilevel finite element model (FE²) is relevant to describe the compressive failure of composite. Furthermore, fiber local buckling leads to a loss of ellipticity of the macroscopic model, which can be a criterion of failure.

Keywords: Asymptotic numerical method, Nonlinear homogenization, Multiscale finite element method, Long fiber composite, Microbuckling, Loss of ellipticity

*Correspondence to Michel Potier-Ferry

Email address: michel.potier-ferry@univ-lorraine.fr (Michel Potier-Ferry)

1. Introduction

It was long believed that the strength of long fiber composite is lower in compression than in tension [1, 2, 3]. This was mainly observed in pure compression tests, but flexural or buckling tests highlighted higher strength level than in tension or pure compression [4, 5, 6]. In other words, compressive strength is not only a material property, but it depends on structural data like specimen size, stacking sequences of composite laminates or loading conditions. In the same spirit, it was experimentally established that a single carbon fiber embedded in an epoxy resin is able to bear higher compressive stress than in tension [7]. One can also mention that the reliability of some pure compression tests is questionable. For instance, the GARTEUR program pointed out that experimental strength depends strongly on the experimental set up [8], which was corroborated by finite element studies, see for instance [9]. In other words, the compressive strength cannot be defined without knowledge of structural data.

Besides, it is well known that compressive strength is governed by an instability called fiber microbuckling [10]. Fiber microbuckling is a local instability that depends mainly on fiber volume fraction, on nonlinearity of matrix behavior in shear and on fiber waviness [11, 12], i.e. on microstructural data. Explicit critical stresses established from a kink band analysis are available [12, 13], which can be corroborated by microstructural finite element computations, see for instance [14, 15]. One can refer for instance to [6, 14, 15, 16, 17, 18, 19, 20] for a full bibliography on the topics.

Hence, a consistent model should involve macroscopic data at the scale of the structure and microscopic data at the scale of the fiber and of the microbuckling wavelength. The model of Drapier et al [21, 16] is a partial answer because it accounts both for microscopic and macroscopic data, but it is limited to few wavelengths and cannot be applied directly to the whole structure. A common criticism can be done to these various local [13, 14, 15] or semi-local [16] modeling: they propose maximal values of the stress from microstructural instability analyses, but it is implicitly assumed that this macroscopic stress is not influenced by the local instability. Concurrent models are nowadays available, for instance the multilevel finite element technique (FE²) also called computational homogenization [22, 23, 24] that considers two nested continuum models needing constitutive assumptions only at the local level. Such a concurrent modeling will be applied in this paper.

Therefore, a consistent numerical modeling of compressive strength has

to involve a double scale analysis, by coupling instabilities at microscopic level with a structural analysis. There are many papers about instability phenomena in heterogeneous materials. In the first one by Abeyaratne and Triantafyllidis (1984) [25] about porous materials, it was found that the homogenized material may lose ellipticity while the matrix remains elliptic. Other papers [26, 27] established a strong connection between macroscopic loss of ellipticity and bifurcation buckling at the local level. Nezamabadi et al. [28, 29] studied the compressive behavior of long fiber composite structures in a FE^2 framework and proved a similar connection between bifurcation at the local level and maximal macroscopic loading. Additional studies can be found in [27, 30, 31, 32, 33, 34, 35, 36, 37].

In the present paper, the same FE^2 approach as in [28, 29] will be used to discuss the connection between local bifurcation, loss of ellipticity at the macroscopic scale and the kink band stress proposed by Budiansky [13]. It is quite well known that the ellipticity condition is related to the stability of a continuous medium and is a necessary condition for the well-posedness of a boundary value problem [38]. Loss of ellipticity is considered as a failure criterion, see for instance [39, 40] that has been used in multi-scale frameworks [30, 33, 35]. Only the classical first gradient continuum model will be considered at the macroscopic level. This is a bit restrictive because the account of fiber bending stiffness is necessary to predict the microbuckling wavelength [41], which should require a model with an internal length such as Cosserat theory [42, 43] or second order homogenization [44].

The paper is organized as follows: in section 2, our multiscale models [28, 29] will be shortly described, the connection between local instability and macroscopic loss of ellipticity will be explained and two classical failure criteria will be presented. Section 3 is devoted to numerical applications. Several multilevel numerical applications will be discussed, especially beam bending tests that can be considered as reference cases [6]. This permits us to revisit the relation between microbuckling, macroscopic loss of ellipticity, mesh sensitivity and kink band predictions, in a multiscale framework with a single constitutive assumption at the microscopic level.

2. Failure model of long fiber composites

2.1. A generic computational homogenization

Let us describe the main features of a multilevel finite element scheme (FE^2) that is also often called computational homogenization. Such a model

is described by two nested domains, each material point belonging together to the so-called macroscopic domain Ω and to a microscopic domain ω , also called Representative Volume Element (RVE) or basic cell. Here both domains are in their reference configuration. After the finite element discretization, each domain is associated to a mesh so that a microscopic domain (or a microscopic mesh) is associated with each integration point of Ω . According to [45], FE² models are characterized by the lack of constitutive law at the macroscopic level and by the localization/homogenization relations. In the case of heterogeneous hyperelastic materials, the multilevel model is represented in Fig. 1 and Table 1, where all macroscopic quantities are denoted by $(\bar{\cdot})$. Classically $\bar{\mathbf{F}} = \nabla \bar{\mathbf{u}} + \mathbf{I}$, is the macroscopic deformation tensor, $\bar{\mathbf{u}}$ denotes the macroscopic displacement field and $\bar{\mathbf{P}}$ is the first macroscopic Piola-Kirchhoff stress tensor. The corresponding quantities at the microscopic level are denoted as \mathbf{F} , \mathbf{u} and \mathbf{P} , while $\boldsymbol{\gamma}$ and \mathbf{S} represent the Green-Lagrange strain and the second Piola-Kirchhoff stress tensor.

The equations (4–8) and the associated boundary conditions define the microscopic problem that is a classical boundary value problem within hyperelasticity. This problem is a function of the macroscopic deformation $\bar{\mathbf{F}}$. Classically, the homogenization relation (2) defines the macroscopic stress as a function of the microscopic stress, so that the problem (2–8) can be considered as a hyperelastic constitutive law at the macroscopic level, the macroscopic stress $\bar{\mathbf{P}}$ depending on the corresponding deformation gradient $\bar{\mathbf{F}}$. This dependence is not represented by a closed-form relation and it follows from the solution of a hyperelastic microscopic problem.

The microscopic problem brings back few questions. The first question is related to the boundary conditions on the RVE that were widely discussed in the literature. Here, we apply the classical periodicity conditions that proved to have least drawbacks. The definition of the RVE is also not simple in the case of microscopic instabilities, even with a periodic spatial distribution, as pointed out in Geymonat et al. [27]. In this paper, we focus on a third question: the non-uniqueness of the solution of the local hyperelastic problem. Since a path following technique will be used, a well-defined family of solutions will be computed that contains solutions along this branch. Nevertheless, there are other solutions and Nezamabadi et al. [28, 29] established numerically that a bifurcation at the microscopic level coincides with a macroscopic maximal load, what is in accordance with the theoretical predictions of Triantafyllidis and Maker[26] associating macroscopic loss of ellipticity and local bifurcation. This question is revisited in this paper.

At the microscopic scale, we assume constitutive relations in each phase (r) of the RVE (see the relation (5)). For the applications that we target in the present work, we shall consider linear material behavior and nonlinear deformation theory

Table 1: Macroscopic and microscopic variational formulations

Macroscopic problem:

$$\int_{\Omega} {}^t\bar{\mathbf{P}} : \delta\bar{\mathbf{F}} \, d\Omega = \lambda \int_{\partial\Omega_t} \mathbf{f} \cdot \delta\bar{\mathbf{u}} \, d\Gamma \quad \text{in } \Omega \quad (1)$$

$$\bar{\mathbf{P}} = \langle \mathbf{P} \rangle = \frac{1}{|\omega|} \int_{\omega} \mathbf{P} \, d\omega \quad (2)$$

$$+ \text{BC: } \bar{\mathbf{u}} = \hat{\mathbf{u}} \quad \text{on } \partial\Omega_u \quad (3)$$

Microscopic problem:

$$\int_{\omega} {}^t\mathbf{P} : \delta\mathbf{F} \, d\omega = 0 \quad (4)$$

$$\mathbf{S} = \mathcal{F}^{(r)}(\boldsymbol{\gamma}) \quad (5)$$

$$\mathbf{P} = \mathbf{F}\mathbf{S} \quad (6)$$

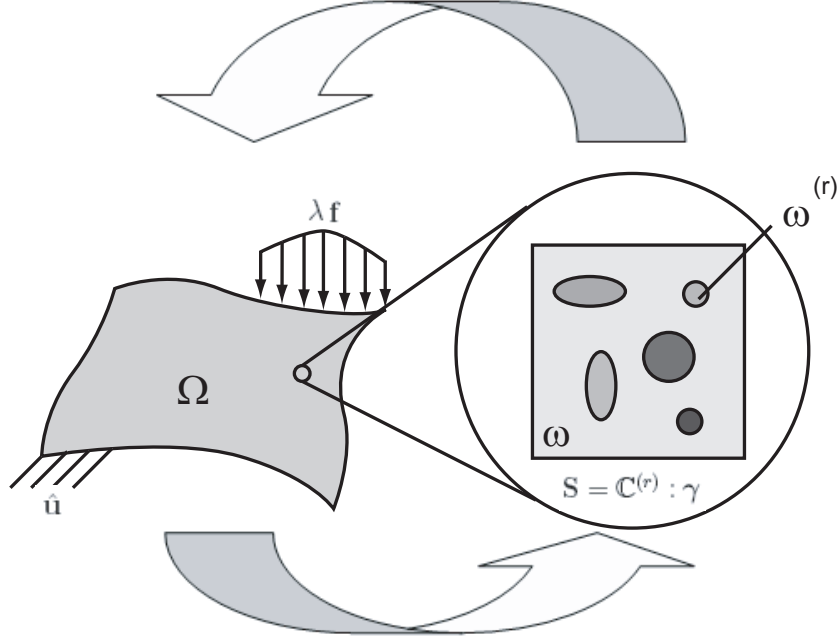
$$\boldsymbol{\gamma} = \frac{1}{2} ({}^t\mathbf{F}\mathbf{F} + \mathbf{I}) \quad (7)$$

$$\mathbf{F} = \boldsymbol{\nabla} \mathbf{u} + \mathbf{I} \quad (8)$$

$$\text{Periodic boundary condition on } \partial\omega : \mathbf{u}^+ - \mathbf{u}^- = (\bar{\mathbf{F}} - \mathbf{I})(\mathbf{X}^+ - \mathbf{X}^-) \quad (9)$$

$$\begin{array}{ll} \text{macroscopic problem} & \text{microscopic problem} \\ \int_{\Omega} {}^t\bar{\mathbf{P}} : \delta\bar{\mathbf{F}} \, d\Omega = \lambda \int_{\partial\Omega_t} \mathbf{f} \cdot \delta\bar{\mathbf{u}} \, d\Gamma & \int_{\omega} {}^t\mathbf{P} : \delta\mathbf{F} \, d\omega = 0 \end{array}$$

$$\bar{\mathbf{P}} = \frac{1}{|\omega|} \int_{\omega} \mathbf{P}(\mathbf{X}) \, d\omega$$



$$\begin{aligned} \bar{\mathbf{F}} &= \frac{1}{|\omega|} \int_{\omega} \mathbf{F}(\mathbf{X}) \, d\omega \\ \mathbf{u}^+ - \mathbf{u}^- &= (\bar{\mathbf{F}} - \mathbf{I})(\mathbf{X}^+ - \mathbf{X}^-) \end{aligned}$$

Figure 1: Computational homogenization scheme

of plasticity [46], both in a finite strain framework. These assumptions are rather common in the studies about compressive strength of composites. These laws are the most simple ones able to capture the main effects, but they are presented only as an example and can be easily modified, for instance to account for elastic unloading. The first law is the linear Saint-Venant Kirchhoff constitutive relation that can be expressed as:

$$\mathbf{S} = \mathbb{C} : \boldsymbol{\gamma} , \quad (10)$$

where \mathbb{C} refers to the classical fourth-order elastic tensor.

Concerning the nonlinear constitutive relation, we choose an elastoplastic constitutive law based on the Ramberg-Osgood relation [47, 48, 49] which is written

in the 3D case in the following form:

$$E \gamma = (1 + \nu) \mathbf{S}^d - (1 - 2\nu) P \mathbf{I} + \frac{3}{2} \alpha \left[\frac{\mathbf{S}_{eq}}{\sigma_y} \right]^{n-1} \mathbf{S}^d, \quad (11)$$

where E , ν , α , n and σ_y denote, respectively, the Young modulus, Poisson's ratio, yield offset, hardening component and the yield stress. $P = -\frac{1}{3} \mathbf{S} : \mathbf{I}$ is the equivalent hydrostatic stress, \mathbf{S}^d is the stress deviator defined by $\mathbf{S}^d = \mathbf{S} + P \mathbf{I}$. \mathbf{S}_{eq} is the von-Mises equivalent stress defined as $\mathbf{S}_{eq} = \sqrt{\frac{3}{2} \mathbf{S}^d : \mathbf{S}^d}$.

2.2. Resolution technique

The full multilevel model is described by the nonlinear system of equations presented in Table 1. The solutions of this nonlinear multiscale problem are sought using the asymptotic numerical method (ANM). ANM is a path following technique where each step is represented by a Taylor series with respect to a path parameter. By comparison with incremental-iterative algorithms, ANM can be considered as a high order predictor without need of any iteration. Many applications of ANM to structural and fluid mechanics show the performance of this technique especially for the treatment of instabilities; see for instance [50, 51, 52, 53]. The problem being coupled, all the variables at the two levels $\mathbf{U} = (\bar{\mathbf{u}}, \bar{\mathbf{P}}, \mathbf{u}, \mathbf{P}, \dots)$ and the load parameter λ are expanded into power series:

$$\left\{ \begin{array}{c} \mathbf{U}(a) \\ \lambda(a) \end{array} \right\} = \left\{ \begin{array}{c} \mathbf{U}_0 \\ \lambda_0 \end{array} \right\} + \sum_{p=1}^N a^p \left\{ \begin{array}{c} \mathbf{U}_p \\ \lambda_p \end{array} \right\}, \quad (12)$$

where $(\cdot)(a)$ refers to quantities defined continuously with respect to a scalar path parameter 'a' to be defined, $(\cdot)_0$ denotes a known initial solution such that $(\cdot)(0) = (\cdot)_0$, N is the truncation order of the series, and $(\cdot)_p$ indicates a term at order 'p' that has to be determined. The resulting problems at each order are linear and can be solved separately at the two levels, as within linear homogenization; but of course, the computation of the full series (12) requires alternate micro/macro computations. It is worth noting that the macroscopic tangent tensor at each macroscopic integration point is computed numerically from constructed problems at the microscopic level. Details of the solving procedure of multiscale problems using ANM are given in our previous papers [28, 29].

We choose the path parameter from the macroscopic displacement field as:

$$a = (\bar{\mathbf{u}}(a) - \bar{\mathbf{u}}_0) \cdot \bar{\mathbf{u}}_1. \quad (13)$$

Note that alternative choices are available, see [54].

Within ANM, each step length is defined a posteriori from the convergence of the series, when all the terms have been computed. This completely adaptive step length is very important to get a secure path following, what is a great help for the present problems involving multiple bifurcations and sudden changes of direction. In this paper, we used a simple end step criterion that is also based on the macroscopic displacement:

$$a_{max} = \left(\delta \frac{\|\bar{\mathbf{u}}_1\|}{\|\bar{\mathbf{u}}_N\|} \right)^{\frac{1}{N-1}} . \quad (14)$$

Thus the algorithm needs only two parameters: the order N that must be sufficiently large to minimize the error of truncation and the accuracy parameter δ that must be very small in order to remain clearly inside the domain of convergence.

2.3. Loss of ellipticity, homogenization and failure of composite

The connection between macroscopic loss of ellipticity and microbuckling is well established and has been discussed from a lot of points of view. This can be explained in a very simple way by considering the classical stack of soft and hard layers as in Fig. 2, the fibers being parallel to Ox_1 . Let us deduce the incremental problem from the balance equation (1) and from $\bar{\mathbf{P}} = \bar{\mathbf{F}}\bar{\mathbf{S}}$. In the small strain case ($\bar{\mathbf{F}}_0 \approx \mathbf{I}$ and $\bar{\mathbf{S}} \approx \bar{\boldsymbol{\sigma}}$ where $\bar{\boldsymbol{\sigma}}$ is the macroscopic Cauchy stress tensor), with a uniaxial pre-stress ($\bar{\mathbf{S}}_0 = \Sigma_0 \mathbf{e}_1 \otimes \mathbf{e}_1$) and with a constant load ($\dot{\lambda} = 0$), it can be written as

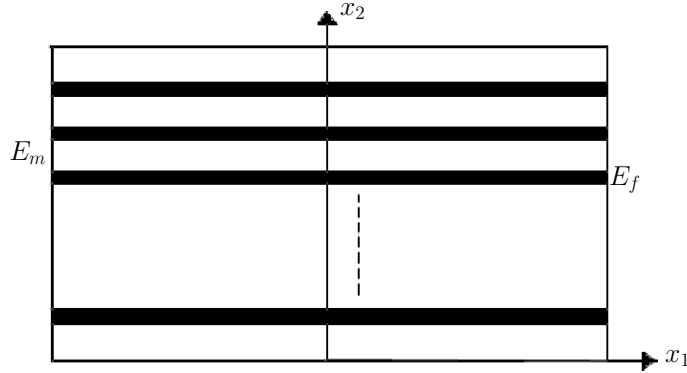


Figure 2: Composite geometry.

$$\int_{\Omega} \left(\dot{\boldsymbol{\sigma}} : \delta \bar{\mathbf{F}} + \Sigma_0 \frac{\partial \dot{\mathbf{u}}}{\partial x_1} \cdot \frac{\partial \delta \bar{\mathbf{u}}}{\partial x_1} \right) d\Omega = 0 , \quad (15)$$

which leads to the classical bifurcation equation:

$$\nabla \cdot \dot{\boldsymbol{\sigma}} + \Sigma_0 \frac{\partial^2 \dot{\mathbf{u}}}{\partial x_1^2} = 0 . \quad (16)$$

The balance equation (16) has to be completed by constitutive equations. In the present small strain framework, elastic homogenization can be performed analytically because of the simplicity of the basic cell. Very simple formulae can be obtained if one considers assumptions that are rather realistic for usual composites, except matrix elasticity that can be removed in forthcoming applications: fiber and matrix are elastic and isotropic, fiber is stiffer than matrix ($E_f \gg E_m$) and Poisson's ratio can be neglected. Indeed, the local equilibrium in the basic cell implies that the transverse and shear stresses are the same in the fiber and in the matrix (i.e. $\sigma_{12} = \bar{\sigma}_{12}$ and $\sigma_{22} = \bar{\sigma}_{22}$), while the axial strain is constant in the basic cell because of the continuity of the displacement along the interface (i.e. $\epsilon_{11} = \bar{\epsilon}_{11}$). Hence, the simplified homogenized constitutive equations can be written as

$$\dot{\sigma}_{11} \approx f E_f \dot{\epsilon}_{11} = f E_f \frac{\partial \dot{u}_1}{\partial x_1} , \quad (17)$$

$$\dot{\sigma}_{12} \approx 2 \frac{G_m}{1-f} \dot{\epsilon}_{12} = \frac{G_m}{1-f} \left(\frac{\partial \dot{u}_1}{\partial x_2} + \frac{\partial \dot{u}_2}{\partial x_1} \right) . \quad (18)$$

$$\dot{\sigma}_{22} \approx \frac{E_m}{1-f} \dot{\epsilon}_{22} = \frac{E_m}{1-f} \frac{\partial \dot{u}_2}{\partial x_2} , \quad (19)$$

where G_m is the matrix shear modulus and $G = \frac{G_m}{1-f}$ is the composite shear modulus. By combining (16–19), one gets a system of linear partial differential equations:

$$(f E_f + \Sigma_0) \frac{\partial^2 \dot{u}_1}{\partial x_1^2} + \frac{G_m}{1-f} \left(\frac{\partial^2 \dot{u}_1}{\partial x_2^2} + \frac{\partial^2 \dot{u}_2}{\partial x_1 \partial x_2} \right) = 0 , \quad (20)$$

$$\left(\frac{G_m}{1-f} + \Sigma_0 \right) \frac{\partial^2 \dot{u}_2}{\partial x_1^2} + \frac{G_m}{1-f} \frac{\partial^2 \dot{u}_1}{\partial x_1 \partial x_2} + \frac{E_m}{1-f} \frac{\partial^2 \dot{u}_2}{\partial x_2^2} = 0 , \quad (21)$$

The system (20–21) is elliptic for a small applied stress Σ_0 , and it loses ellipticity when the first term of (21) vanishes, i.e. when:

$$\Sigma_0 = - \frac{G_m}{1-f} = -G . \quad (22)$$

Thus this ellipticity-homogenization approach permits to recover the microbuckling critical load of Rosen [10] that was established by a linear bifurcation analysis, where the fiber was represented by a flexible beam and the shear stress is dominant

in the matrix. Thus a simple multilevel model is able to highlight the coincidence between fiber microbuckling and loss of ellipticity at the macroscopic level.

This class of multilevel model should be improved in two ways. First, a classical continuous model as (20–21) is not able to define neither the microbuckling wavelength nor the macroscopic bifurcation mode. This would require accounting both fibers bending as in Rosen model and transverse effects as in the last term of (21), as illustrated in [41, 55]. In the same way, the multilevel model of Table 1 will not be able to represent the bifurcation mode at the macroscopic level: a model with internal length would be necessary for this. On the basis of the first gradient model of Table 1, one can predict the failure level, but not the details of the deformation pattern at the end of the failure process.

Second, it is well known that the critical stress (22) is too high and one has to include nonlinear matrix behavior and fiber waviness to get realistic predictions. Of course this will be accounted easily in our multilevel model of Table 1. Closed-form formulae have been established from nonlinear local kink-band analyses, see [11, 12, 13]. In this paper, we shall discuss the analytic formula of Budiansky and Fleck [13] that follows from a local analysis with a mode in the form of a shear band. It can be expressed as:

$$\sigma_c = \frac{G}{1 + n \left(\frac{3}{7}\right)^{1/n} \left(\frac{\bar{\phi}/\gamma_y^c}{n-1}\right)^{(n-1)/n}}, \quad (23)$$

where G is the elastic shear modulus of the composite, $\bar{\phi}$ is the initial misalignment angle of the kink band, n is the hardening exponent and γ_y^c denotes the yield strain in shear. This formula has been obtained from the assumption of a linear elastic fiber and an elastoplastic matrix according to the deformation theory (11). If no misalignment, the failure strain (23) is equivalent to the Rosen’s microbuckling prediction and to loss of ellipticity condition (22).

In this paper, we aim at defining the failure limit from a multi-level modeling without ad hoc assumptions as in the shear band analysis. In this respect, Hadamard ellipticity is a relevant and universal concept to define the stability domain. It is expressed from the acoustic tensor $\mathbf{Q}(\mathbf{n})$ based on the macroscopic tangent stiffness tensor \bar{L} :

$$Q_{ij} = \bar{L}_{kilj} n_k n_l. \quad (24)$$

In the stability domain, this acoustic tensor is positive definite for any direction \mathbf{n} , $\mathbf{n} \neq 0$. Thus the stability limit can be characterized by:

$$\exists \mathbf{n} \neq 0 \text{ such that } \det(\mathbf{Q}(\mathbf{n})) = 0. \quad (25)$$

In the next section, we shall compare the numerical predictions of the two stability criteria (23) and (25). Even though they seem very different, they express

the same multi-scale instability property as long as the acoustic tensor is defined from a multi-level modeling as in 2.1. Indeed the Budiansky-Fleck formula (23) results from a local instability analysis and it is known that the condition of macroscopic loss of ellipticity (25) generally coincides with a local bifurcation [26, 28]. Obviously the condition (23) has the advantage to be explicit and therefore easily understood and cheap to be applied. As for the condition (25), this is a generic condition to have a well-posed problem, it does not assume a specific mode and does not imply a specific constitutive law that is introduced only at the local level.

3. Numerical examples

In this section, the multi-scale model is applied to several simple structural problems. The constitutive laws are only defined at the local level: the fiber and sometimes the matrix follow the linear Saint-Venant Kirchhoff law. When dealing with more realistic materials, the Ramberg-Osgood model (11) will be considered. No macroscopic constitutive law is needed: this is the main originality of this paper. Of course the FE² multi-scale approach is a generic procedure that can be applied to any material modeling and any microstructural geometry, unlike closed-form formulae like (23) that are simple, but assume a specific imperfection shape and matrix behavior.

The discussion focuses on the failure criterion: as suggested in [25], there is a strong connection between macroscopic loss of ellipticity and bifurcation at the local level. This suggests that loss of ellipticity could be considered as a failure criterion, which has the advantage of being a universal property independent of the model. On the contrary, the classical failure criteria for composite material (see e.g. [13]) involve material and structural properties that are here included in the multi-scale model. The two types of approaches will be compared in the next examples.

The proposed problems have been discretized using two-dimensional finite element in the plane stress framework, at the two scales. The macrostructures have been meshed with eight-node quadrangular elements whereas the microstructures have been meshed with nine-node quadrangular elements. These elements have been used with a 3×3 Gauss integration scheme.

Let us underline a weak point of the approach: the instability wavelength is prescribed via the choice of the width of the unit cell. As highlighted in [27], the periodicity of the response is not necessarily the material periodicity. For one-dimensional microstructures as in Fig. 3, it is possible to deduce the microbuckling wavelength [42], but not in a first gradient approach as here.

The few parameters of the algorithm are the truncation order N of the series and the accuracy parameter δ which allows limiting the length of each asymptotic

step in a continuation procedure. The chosen values of N and δ are about the same as in many other calculations. In all the tests presented here, we have solved the nonlinear problems using ANM with $N = 15$, but $\delta = 10^{-6}$ for the first test and $\delta = 10^{-8}$ for the second one. For all the examples, Poisson's ratio is equal to 0.3.

3.1. Elastic microbuckling of a fiber reinforced structure

The first example is a very simple benchmark already studied in [28]: the fiber is straight and the macroscopic domain is a rectangle (Fig. 3 and 4). We consider periodic boundary conditions on the RVE as described in Table 1. The rigidity ratio of fiber per matrix is equal to 1000 ($E_f/E_m = 1000$ and $E_f = 100000$ MPa). The macrostructure is shown in Fig. 4: it is a rectangular plate clamped on three edges and submitted to a force distribution λP on a part of the top edge. Because of the symmetry of the problem, only a half of the structure is discretized. We use our multiscale procedure to solve this micro-macro problem.

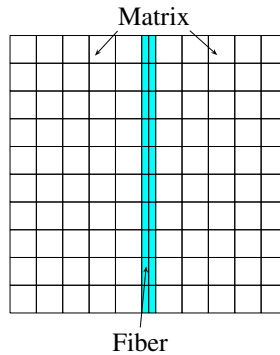


Figure 3: Elementary cell of a fiber reinforced composite material. The fiber is straight, $\frac{h}{l} = \frac{1}{20}$.

To show the mesh dependency of the macroscopic results, we consider three types of mesh shown in Fig. 5. The load-displacement responses for different meshes are presented in Fig. 6 that shows the displacements of the points located on Fig. 5. This figure shows the influence of microscopic instability on the macroscopic one: initially, in the portions of the curves preceding the points of the loss of ellipticity (points LE_1 , LE_2 and LE_3), the macroscopic behavior is mainly linear. However, we can observe an abrupt change after these points. This is caused by the occurrence of microscopic instabilities at these points. It is worth noting that thanks to the high order predictor of ANM, we can detect these instabilities. Moreover, we can observe clearly the macroscopic mesh dependence in this multiscale problem.

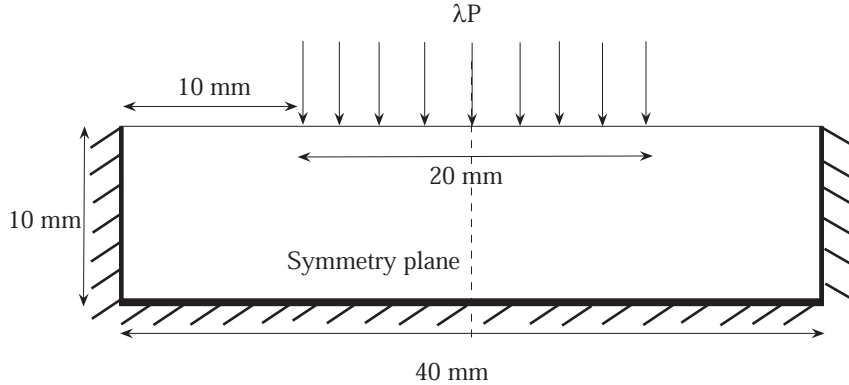


Figure 4: Geometry and boundary conditions of the rectangular plate made of the fiber reinforced composites, $P = 1 \text{ N/mm}$

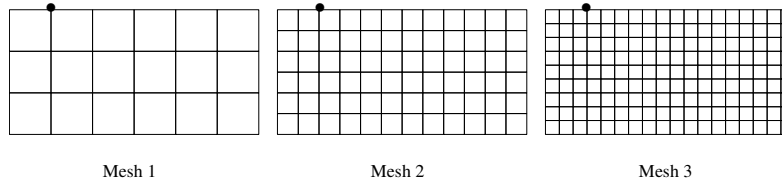


Figure 5: Different macroscopic meshes

Rosen's microbuckling stress (22) is 40.5 MPa in this case. The points corresponding to this stress (points SB_1 , SB_2 and SB_3) are shown in Fig. 6. We observe that the points of the loss of ellipticity are close to these points for all meshes.

Thus in this simple elastic case, the double scale model associated with the Rice-Hadamard criterion permits to recover the predictions of the simplest microbuckling approach. This corroborates many previous results, see for instance [25, 26, 33, 35]. Beyond this limit, the multi-scale model is not well-posed, as shown by the observed mesh dependence. In a previous paper [28], the same problem was solved with another microscopic boundary condition (prescribed displacement). In the latter case, a macroscopic instability characterized by a maximal load point was observed just after the microscopic bifurcation. In the present case, it is not so easy to detect the microscopic instability, at least with a coarse mesh, but the

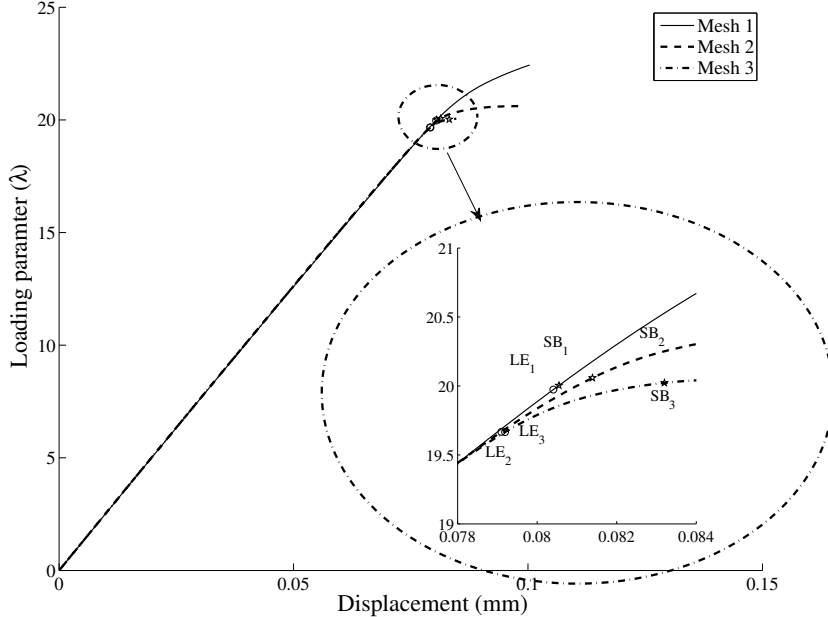


Figure 6: Load-displacement diagrams for different meshes. The multi-scale problem is described in Fig. 3 and 4, with an elastic behavior. One compares the failure levels predicted by loss of ellipticity, pictured by LE and circles (\circ) and by the shear band approach, pictured by SB and by stars (\star).

loss of ellipticity criterion seems to work for any mesh.

3.2. Bending of a beam made of a fiber reinforced composite

After the previous academic test, we try to model more realistic structures. Beam bending tests are among the most simple and the most useful ones to characterize the strength of composite materials, see for instance [5, 6, 9]. One knows that fiber waviness and matrix nonlinear behavior are necessary to get realistic failure predictions [11, 12]: this will be easily introduced in the definition of the microstructural problem. The chosen material properties are issued from experimental data [4] and have been previously used in other models, see for instance [16].

3.2.1. Plastic microbuckling from a multi-scale computation

First let us consider only the microscopic problem by prescribing a uniaxial compressive strain ($\mathbf{F}=F_{11} \mathbf{e}_1 \otimes \mathbf{e}_1$, where \mathbf{e}_1 corresponds to the direction of the

Table 2: Characteristics of T300/914 material and data used for the plastic microbuckling study

Fiber T300 (isotropic)	Matrix 914 (isotropic)	Composite T300/914	Imperfection
$E_f = 230 \text{ GPa}$	$E_m = 4500 \text{ MPa}$	$E = 139800 \text{ MPa}$	$\lambda_0 = 200 \pi \mu\text{m}$
$\nu_f = 0.3$	$G_m = 1600 \text{ MPa}$	$G = 3817 \text{ MPa}$	$v_0 = 3 \mu\text{m}$
$r_f = 5 \mu\text{m}$	$\nu_m = 0.4$		$\phi_0 = 3^\circ$
$f = 0.6$	$n = 3$		
	$\sigma_y^m = 60 \text{ MPa}$		
	$\epsilon_y^m = 2 \%$		

fibers). The goal is to check the ability of the microscopic model to recover basic plastic microbuckling phenomena, for example as in [12, 13, 14, 15, 16]. The employed mechanical properties are shown in table 2, which corresponds to a T300/914 composite. The width of the basic cell is given by the material geometry, but a priori the microbuckling wavelength is not a data. This wavelength can be deduced from a second gradient model as in [41, 55] and a value of $200 \pi \mu\text{m}$ is relevant. We choose the same value for the imperfection wavelength and the length of the basic cell. The fiber is no longer straight: it is sinusoidal and the imperfection magnitude (\mathbf{v}_0) is constant through the thickness. All these geometric data are summarized in the basic cell pictured in Fig. 7. The parameters characterizing the nonlinear behavior of the matrix are deduced from [16].

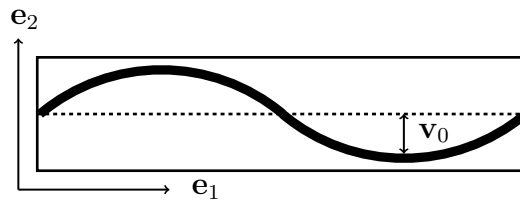


Figure 7: The basic cell with an imperfection of amplitude \mathbf{v}_0 .

Fig. 8 shows the macroscopic constitutive law that is deduced from the plastic computation on the basic cell for various sizes of the imperfection. These results are similar to many results from the literature [14, 15, 16]. For small imperfections, there is a sharp peak and the maximal stress is expected to be close to the loss of ellipticity.

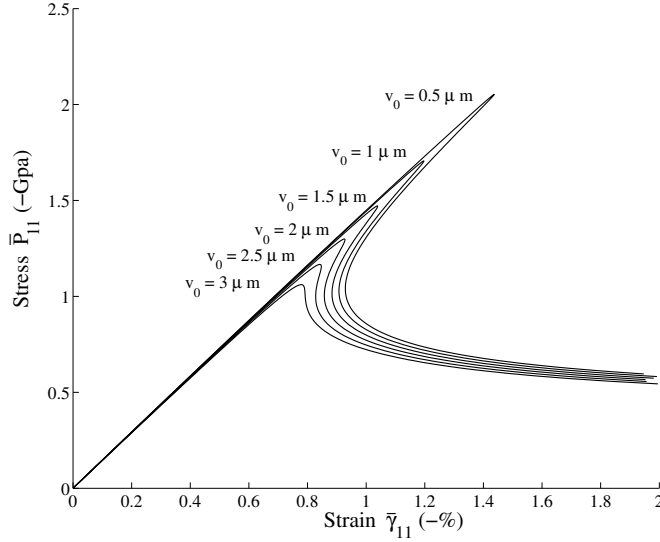


Figure 8: The macroscopic stress-strain diagrams for the different imperfection magnitudes.

3.2.2. Interaction between micro- and macro-instabilities

We now study full structural problems with a constitutive law deduced from a microstructural problem, according to the FE² procedure of section 2.1. The macro-structure is a simply supported beam submitted to three types of force distribution λP on the top edge of the macrostructure (see Fig. 9). The beam has been discretized using 60 (15×4) eight-node quadrangular elements. The microstructure is the same as in the previous part, with an elastic fiber, a plastic matrix and a sinusoidal imperfection $\mathbf{v}_0 = 3 \mu\text{m}$.

The load-displacement responses for the three different cases are presented in Fig. 10 where the displacements of the points located on the top middle of beam are plotted. The failure stresses characterized by the criterion of macroscopic loss of ellipticity are located (points LE₁, LE₂ and LE₃), as well as by the criterion deduced from the shear band analysis (points SB₁, SB₂ and SB₃): clearly the two criteria give very close results, corresponding here to a limit stress of -1030 MPa. Note that the macroscopic mesh dependence also exists in this problem, but the influence of the macroscopic instability is not very apparent in Fig. 10 because of a rather coarse mesh.

Last we underline the connection between local instability and macroscopic loss of ellipticity. In this respect, one has pictured in Fig. 11b the deformed shapes of the microstructure at the integration point located in the top middle (in a $3 \times$

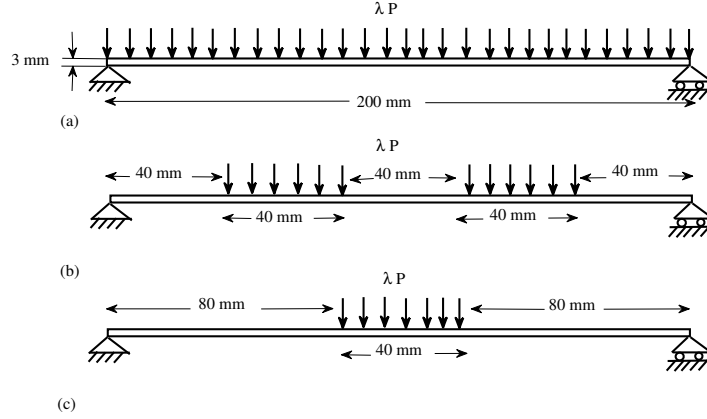


Figure 9: Geometries and boundary conditions of the rectangular beams made of the fiber reinforced composites with different loadings: (a) Loading case 1; (b) Loading case 2; (c) Loading case 3; $P = 1 \text{ N/mm}$

3 integration point scheme) of the top middle element at points A, B and C of the load-displacement curve (see Fig. 11a). There is a significant difference between these deformed microstructural shapes despite the small variation of macroscopic load. The growth of local buckles becomes important at the point B that is near the point of the loss of ellipticity. In Fig. 11c, the macroscopic stress-strain diagram is presented for the considered integration point. The points A, B and C in this figure are the same as in Fig. 11a. Note that the point B corresponds also to the maximum stress (see Fig. 11a and 11c). This illustrates the strong connection between local and global instabilities, between local buckling and loss of ellipticity, between shear band analysis and the present multi-scale approach. The latter point may be surprising because the local modes are not the same: the double scale finite element method predicts more or less sinusoidal mode shapes (see Fig. 11b) that does not look like shear bands.

Finally, let us discuss the sensitivity of the approach to the size of the basic cell. Theoretically any buckling analysis depends on the size of the body; but, in this case, this dependence should be rather weak: for instance the Rosen microbuckling stress (22) is not length-dependent. The FE^2 calculation of Fig. 11 has been done for three values of the microscopic length: $\lambda_0 = 200 \pi \mu\text{m}$, $\lambda_0 = 150 \pi \mu\text{m}$, $\lambda_0 = 100 \pi \mu\text{m}$. The corresponding loss of ellipticity occurs respectively for a stress of -1030 MPa, -1050 MPa, -1025 MPa, which confirms the weak dependence to the microstructural length.

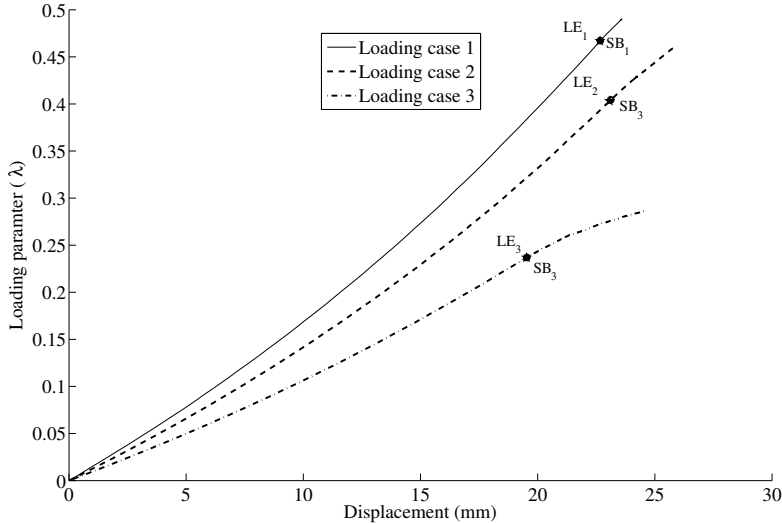


Figure 10: The load-displacement diagrams of the plastic microbuckling problem for different loading cases. The circles (\circ) are the points of the loss of ellipticity and the stars (\star) denote the points corresponding to the theoretical failure compressive stress.

4. Conclusion

The present paper has been devoted to investigate the compressive failure of long fiber composites, thanks to a multiscale finite element procedure. This technique combines multiscale finite element analysis (FE^2) and asymptotic numerical method (ANM). Several numerical tests have proved the relevance of the concept of macroscopic loss of ellipticity to define a compressive failure criterion. The strong connection between macroscopic loss of ellipticity and bifurcation at the local level has been long established [25]. This has been confirmed in this paper from multiscale finite element calculations. Moreover, the predictions obtained by a well-established shear band analysis are very close to those obtained by combining multiscale finite element and loss of ellipticity. Thus it appears that this combination between loss of ellipticity and FE^2 leads to a relevant and clear failure criterion. Because the macroscopic model becomes ill-posed beyond, this approach does not permit to predict the last stages of the failure process, which would require a macroscopic model with an internal length, for instance as in [45]. Clearly the double scale concurrent approach leads to high computational costs and that is why we limited ourselves to 2D models. Likely it would be possible to consider more simple modeling, for example by coming back to an uncoupled approach or

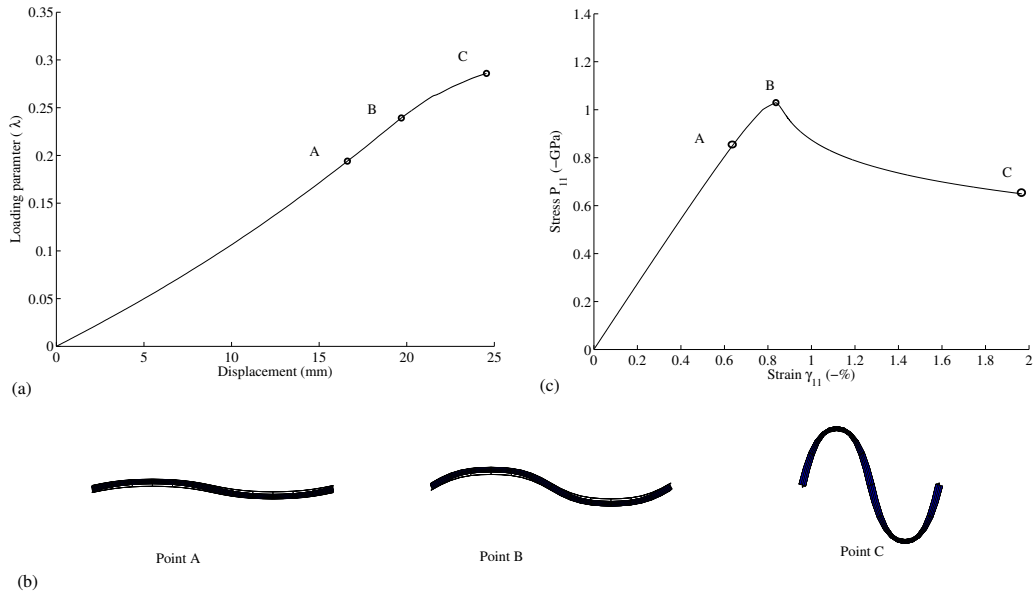


Figure 11: Third loading case: (a) The load-displacement diagram; (b) Deformed shapes of microstructure at the integration point located in the top middle (in a 3×3 integration point scheme) of the top middle element at points A, B and C, deformation scale = 10;(c) The macroscopic stress-strain diagram for the considered integration point.

by applying reduced-order models at the local level.

5. Acknowledgements

Michel Potier-Ferry and Hamid Zahrouni gratefully acknowledge the financial support of the French National Research Agency ANR (Labex DAMAS, Grant No. ANR-11-LABX-0008-01).

References

- [1] A. M. Waas, C. D. Babcock Jr, W. G. Knauss, An experimental study of compression failure of fibrous laminated composites in the presence of stress gradients, *International Journal of Solids and Structures* 26 (1990) 1071–1098.
- [2] C. Soutis, N. A. Fleck, P. A. Smith, Failure prediction technique for compression loaded carbon fibre-epoxy laminate with open holes, *Journal of Composite Materials* 25 (1991) 1476–1498.

- [3] A. M. Waas, Failure criteria for composites, Tech. Rep. ADA383128, University of Michigan, Aerospace Engineering Department, Ann Arbor (1999).
- [4] M. R. Wisnom, The effect of specimen size on the bending strength of unidirectional carbon fibre-epoxy, *Composite Structures* 18 (1991) 47–63.
- [5] I. Grandsire-Vincon, Compression des composites unidirectionnels: Méthodes d’essais et approche micromécanique, Ph.D. thesis, ENS, Cachan, FRANCE (1993).
- [6] M. R. Wisnom, Size effects in the testing of fibre-composite materials, *Composites Science and Technology* 59 (1999) 1937–1957.
- [7] I. Vincon, O. Allix, P. Sigety, M. H. Auvray, Compressive performance of carbon fibres: experiment and analysis, *Composites science and technology* 58 (1998) 1649–1658.
- [8] W. J. G. Hart, R. Aoki, H. Bookholt, P. Curtis, I. Krober, N. Marks, P. Sigety, Garteur compression behaviour of advanced CRFP, in: AGARD Report 785. The utilisation of advanced composites in military aircraft. 73rd meeting of the AGRAD structures and materials panel held in San Diego, 1991.
- [9] O. Anthoine, J. C. Grandidier, L. Daridon, Pure compression testing of advanced fibre composites, *Composite science and technology* 58 (1998) 735–740.
- [10] B. W. Rosen, Mechanics of composite strengthening, *Fiber composite materials*, American Society for Metals Seminar 3 (1964) 37–75.
- [11] A. S. Argon, Fracture of composites, *Treatise of Materials Science and Technology*, Vol. 1, Academic Press, New York, 1972.
- [12] B. Budiansky, Micromechanics, *Computers & Structures* 16 (1983) 3–12.
- [13] B. Budiansky, N. A. Fleck, Compressive failure of fibre composites, *Journal of the Mechanics and Physics of Solids* 41 (1993) 183–211.
- [14] S. Kyriakides, R. Arseculeratne, E. J. Perry, K. M. Liechti, On the compressive failure of fiber-reinforced composites, *International Journal of Solids and Structures* 32 (1995) 689–738.
- [15] S. H. Lee, A. M. Waas, Compressive response and failure of fiber reinforced unidirectional composites, *International Journal of Fracture* 100 (1999) 275–306.

- [16] S. Drapier, J. C. Grandidier, M. Potier-Ferry, A structural approach of plastic microbuckling in long fibre composites: comparison with theoretical and experimental results, *International Journal of Solids and Structures* 38 (2001) 3877–3904.
- [17] X. Martinez, S. Oller, Numerical simulation of matrix reinforced composite materials subjected to compression loads, *Archives of Computational methods in Engineering* 16 (2009) 357–397.
- [18] S. L. Lemanski, M. P. F. Sutcliffe, Compressive failure of finite size unidirectional composite laminates with a region of fibre waviness, *Composites Part A: Applied Science and Manufacturing* 45 (2012) 435–444.
- [19] N. Feld, O. Allix, E. Baranger, J. M. Guimard, A micromechanics-based mesomodel for unidirectional laminates in compression up to failure, *Journal of Composite Materials* 46 (2012) 2893–2909.
- [20] J. C. Grandidier, P. Casari, C. Jochum, A fibre direction compressive failure criterion for long fibre laminates at ply scale, including stacking sequence and laminate thickness effects, *Composite Structures* 49 (2012) 3799–3806.
- [21] S. Drapier, J. C. Grandidier, M. Potier-Ferry, Towards a numerical model of the compressive strength for long fibre composites, *European journal of mechanics. A. Solids* 18 (1999) 69–92.
- [22] M. Gologanu, J. B. Leblond, G. Perrin, J. Devaux, Recent extensions of gurgon’s model for porous ductile metals, in: P. Suquet (Ed.), *Continuum Micromechanics*, CISM Lectures Series, Springer, New York, 1997, pp. 61–130.
- [23] R. J. M. Smit, W. A. M. Brekelmans, H. E. H. Meijer, Prediction of the mechanical behavior of nonlinear heterogeneous systems by multi-level finite element modeling, *Computer Methods in Applied Mechanics and Engineering* 155 (1998) 181–192.
- [24] F. Feyel, J. L. Chaboche, FE^2 multiscale approach for modeling the elastoviscoplastic behavior of long fiber SiC/Ti composite materials, *Computer Methods in Applied Mechanics and Engineering* 183 (2000) 309–330.
- [25] R. Abeyaratne, N. Triantafyllidis, An investigation of localization in a porous elastic material using homogenization theory, *Journal of Applied Mechanics* 51 (1984) 481–486.

- [26] N. Triantafyllidis, B. N. Maker, On the comparison between microscopic and macroscopic instability mechanisms in a class of fiber-reinforced composites, *Journal of Applied Mechanics* 52 (1985) 794–800.
- [27] G. Geymonat, S. Müller, N. Triantafyllidis, Homogenization of nonlinearly elastic materials: microscopic bifurcation and macroscopic loss of rank-one convexity, *Archive for Rational Mechanics and Analysis* 122 (1993) 231–290.
- [28] S. Nezamabadi, J. Yvonnet, H. Zahrouni, M. Potier-Ferry, A multilevel computational strategy for microscopic and macroscopic instabilities, *Computer Methods in Applied Mechanics and Engineering* 198 (2009) 2099–2110.
- [29] S. Nezamabadi, H. Zahrouni, J. Yvonnet, M. Potier-Ferry, A multiscale finite element approach for buckling analysis of elastoplastic long fiber composites, *International Journal for Multiscale Computational Engineering* 8 (2010) 287–301.
- [30] N. Ohno, D. Okumura, H. Noguchi, Microscopic symmetric bifurcation condition of cellular solids based on a homogenization theory of finite deformation, *Journal of the Mechanics and Physics of Solids* 52 (2002) 1125–1153.
- [31] C. Miehe, J. Schröder, M. Becker, Computational homogenization analysis in finite elasticity: material and structural instabilities on the micro- and macro-scales of periodic composites and their interactions, *Computer Methods in Applied Mechanics and Engineering* 191 (4) (2002) 4971–5005.
- [32] L. Gong, S. Kyriakides, N. Triantafyllidis, On the stability of Kelvin cell foams under compressive loads, *Journal of the Mechanics and Physics of Solids* 53 (2005) 771–794.
- [33] O. Lopez-Pamies, P. Ponte Castañeda, Second-order estimated for the macroscopic response and loss of ellipticity in porous rubbers at large deformations, *Journal of Elasticity* 76 (2005) 247–287.
- [34] G. deBotton, I. Hariton, E. A. Socolsky, Neo-Hookean fiber reinforced composites in finite elasticity, *Journal of the Mechanics and Physics of Solids* 54 (2006) 533–559.
- [35] J. C. Michel, O. Lopez-Pamies, P. Ponte Castañeda, N. Triantafyllidis, Microscopic and macroscopic instabilities in finitely strained porous elastomers, *Journal of the Mechanics and Physics of Solids* 55 (2007) 900–938.

- [36] J. Yvonnet, H. Zahrouni, M. Potier-Ferry, A model reduction method for the post-buckling analysis of cellular microstructures, *Computer Methods in Applied Mechanics and Engineering* 197 (2007) 265–280.
- [37] D. Okumura, A. Okada, N. Ohno, Buckling behavior of Kelvin open-cell foams under $[0\ 0\ 1]$, $[0\ 1\ 1]$ and $[1\ 1\ 1]$ compressive loads, *International Journal of Solids and Structures* 45 (2008) 3807–3820.
- [38] J. Hadamard, *Lecons sur la Propagation des Ondes*, Hermann et Cie, Paris, France, 1903.
- [39] J. W. Rudnicki, J. R. Rice, Conditions for the localization of deformation in pressure-sensitive dilatant materials, *Journal of the Mechanics and Physics of Solids* 23 (1975) 371–394.
- [40] J. R. Rice, The localization of plastic deformation, in: W. T. Koiter (Ed.), *Theoretical and Applied Mechanics (Proceedings of the 14th International Congress on Theoretical and Applied Mechanics)*, Delft, Netherlands, 1976, pp. 207–220.
- [41] J. C. Grandidier, G. Ferron, M. Potier-Ferry, Microbuckling and strength in long-fiber composites - theory and experiments, *International Journal of Solids and Structures* 29 (1992) 1753–1761.
- [42] N. A. Fleck, J. Y. Shu, Microbuckle initiation in fibre composites: a finite element study, *Journal of the Mechanics and Physics of Solids* 43 (1995) 1887–1918.
- [43] S. Forest, K. Sab, Cosserat overall modeling of heterogeneous materials, *Mechanics Research Communications* 25 (1998) 449–454.
- [44] V. G. Kousnetzova, M. G. D. Geers, W. A. M. Brekelmans, Multi-scale constitutive modelling of heterogeneous materials with a gradient-enhanced computational homogenization scheme, *International Journal for Numerical Methods in Engineering* 54 (2002) 1235–1260.
- [45] F. Feyel, A multilevel finite element method (FE^2) to describe the response of highly non-linear structures using generalized continua, *Computer Methods in Applied Mechanics and Engineering* 192 (2003) 3233–3244.
- [46] H. Hencky, Zur theorie deformationen und der hierdurch im material hervorgerufenen nebenspannungen, *Zeitschrift Für Angewandte mathematik und Mechanik* 4 (1924) 323–334.

- [47] W. F. Chen, D. J. Han, Plasticity for structural engineers, Springer-Verlag, New York, 1998.
- [48] ABAQUS, Theory manual, version 6.8, Hibbit, Karlsson and Sorensen Inc. (2008).
- [49] H. Zahrouni, M. Potier-Ferry, H. Elasmay, N. Damil, Asymptotic numerical method for nonlinear constitutive laws, *Revue Européenne des Eléments Finis* 7 (1998) 841–869.
- [50] B. Cochelin, A path following technique via an asymptotic numerical method, *Computers and Structures* 53 (1994) 1181–1192.
- [51] H. Zahrouni, B. Cochelin, M. Potier-Ferry, Computing finite rotations of shells by an asymptotic numerical method, *Computer Methods in Applied Mechanics and Engineering* 175 (1999) 71–85.
- [52] J. M. Cadou, B. Cochelin, M. Potier-Ferry, A numerical method for the computations of bifurcation points in fluid mechanics, *European Journal of Mechanics-B* 25 (2006) 234–254.
- [53] B. Cochelin, N. Damil, M. Potier-Ferry, *Méthode asymptotique numérique*, Hermès Science Publications, 2007.
- [54] H. Mottaqui, B. Braikat, N. Damil, Discussion about parameterization in the asymptotic numerical method: Application to nonlinear elastic shells, *Computer Methods in Applied Mechanics and Engineering* 199 (2010) 1701–1709.
- [55] S. Drapier, J. C. Grandidier, M. Potier-Ferry, Structure effect and microbuckling, *Composites science and technology* 56 (1996) 861–867.